

METHODS PAPER  

Sinh-arcsinh-normal distributions to add uncertainty to neural network regression tasks: Applications to tropical cyclone intensity forecasts

Elizabeth A. Barnes¹ , Randal J. Barnes²  and Mark DeMaria³ 

¹Department of Atmospheric Science, Colorado State University, Fort Collins, CO, USA

²Department of Civil, Environmental, and Geo- Engineering, University of Minnesota, Minneapolis, MN, USA

³Cooperative Institute for Research in the Atmosphere, Colorado State University, Fort Collins, CO, USA

Corresponding author: Elizabeth A. Barnes; Email: eabarnes@colostate.edu

Received: 11 July 2022; **Revised:** 02 May 2023; **Accepted:** 08 May 2023

Keywords: Machine learning; neural networks; Sinh-arcsinh-normal distribution; tropical cyclones; uncertainty quantification

Abstract



A simple method for adding uncertainty to neural network regression tasks in earth science via estimation of a general probability distribution is described. Specifically, we highlight the sinh-arcsinh-normal distributions as particularly well suited for neural network uncertainty estimation. The methodology supports estimation of heteroscedastic, asymmetric uncertainties by a simple modification of the network output and loss function. Method performance is demonstrated by predicting tropical cyclone intensity forecast uncertainty and by comparing two other common methods for neural network uncertainty quantification (i.e., Bayesian neural networks and Monte Carlo dropout). The simple approach described here is intuitive and applicable when no prior exists and one just wishes to parameterize the output and its uncertainty according to some previously defined family of distributions. The authors believe it will become a powerful, go-to method moving forward.

Impact Statement

Uncertainty quantification via machine learning is a vibrant area of research, and many methods have been proposed. Here, we describe and demonstrate a simple method for adding uncertainty to most any neural network (a type of machine learning algorithm) regression task. We demonstrate the utility of this method by predicting tropical cyclone intensity forecast uncertainty. The method is intuitive and straightforward to implement with standard machine learning software. The authors believe it will become a powerful, go-to method moving forward.

1. Introduction

Uncertainty quantification via machine learning methods is a vibrant area of research (e.g., Sensoy et al., 2018; Amini et al., 2019), and many methods for uncertainty estimation via artificial neural networks have been proposed (e.g., Abdar et al., 2021; Jospin et al., 2022). Many studies have focused on uncertainty

  This research article was awarded Open Data and Open Materials badges for transparent practices. See the Data Availability Statement for details.

© The Author(s), 2023. Published by Cambridge University Press. This is an Open Access article, distributed under the terms of the Creative Commons Attribution licence (<http://creativecommons.org/licenses/by/4.0>), which permits unrestricted re-use, distribution and reproduction, provided the original article is properly cited.

quantification for classification; however, problems in the earth sciences are often framed in terms of regression tasks (i.e., estimating continuous values). For example, scientists might wish to estimate how much it will rain tomorrow, the peak discharge of a river next year, or the thickness of an aquifer at a set of locations. Estimates of the uncertainty associated with the predicted values are necessary to formulate policy, make decisions, and assess risk.

Here, we describe and demonstrate a simple method for adding uncertainty to most any neural network regression architecture. The method works by tasking the network to locally predict the parameters of a user-specified probability distribution, rather than just predict the value alone. Although the approach was introduced decades ago (Nix and Weigend, 1994, 1995) and is a standard in the computer science literature (e.g., Sountsov et al., 2019; Duerr et al., 2020), it is much less known in the earth science community. A few applications of the method appear in the recent literature (e.g., Barnes and Barnes, 2021; Foster et al., 2021; Guillaumin and Zanna, 2021; Gordon and Barnes, 2022), but all of these focus strictly on the Gaussian distribution.

The Gaussian distribution has the benefits of familiarity and the comforts of common use. Nonetheless, the Gaussian distribution is sorely limiting due to its symmetry and fixed tailweight. In the earth sciences, uncertainty is often asymmetric. Consider the prediction of strictly positive quantities such as rain intensity, stream discharges, contaminant concentrations, and wind speeds. There is a chance that the true value is greater than twice the predicted value, but there is never any chance that the true value is less than zero.

Here, we formulate neural network regression with uncertainty quantification using the sinh-arcsinh-normal distribution (Jones and Pewsey, 2009, 2019). While two parameters define a Gaussian distribution (location and scale), the sinh-arcsinh-normal distribution is defined by four parameters (location, scale, skewness, and tailweight). This method for incorporating uncertainty with the sinh-arcsinh-normal distribution (which we call SHASH) is understandable, surprisingly general, and simple to implement with confidence. The sinh-arcsinh-normal distribution is certainly not the only choice of distribution for environmental problems, and in fact, there may be better-suited distributions depending on the specific application. Here, we merely wish to demonstrate the utility of the sinh-arcsinh-normal distribution for capturing asymmetric uncertainties in predicting hurricane intensity errors. Overall, we believe that this simple method for adding uncertainty using a user-defined distribution will become a powerful go-to approach moving forward.

2. Data

The data set for this study is based on how forecasters at the National Weather Service (NWS) National Hurricane Center (NHC) in Miami make their subjective forecasts of the tropical cyclone maximum sustained surface wind (intensity) out to 5 days. Several objective models provide intensity forecast guidance, and verification results show that the equally weighted consensus of the best-performing individual models is often the most accurate (Cangialosi, 2022). The consensus model (Consensus from here on out) provides a first-guess intensity; then forecasters will lean their forecast more toward individual models they feel best handle the tropical cyclone based on the current forecast situation.

For the 2021 Hurricane Season, NHC's primary equally weighted intensity consensus model (IVCN) consisted of the following five forecast models: (1) The Decay-Statistical Hurricane Intensity Prediction Scheme (DSHP); (2) The Logistic Growth Equation Model (LGEM); (3) The Hurricane Weather Research and Forecast Model (HWRF); (4) The Hurricanes in a Multiscale Ocean-coupled Non-hydrostatic (HMON) Model; and (5) The U.S. Navy's Coupled Ocean-Atmosphere Mesoscale Prediction System for tropical cyclones (CTCX). LGEM and D-SHIPS are statistical-dynamical models, while HWRF, HMON, and CTCX are regional dynamical models. Although not included in IVCN, intensity forecasts from several global models, such as the National Weather Service Global Forecasting System (GFS), are also used for the NHC official forecast. Cangialosi et al. (2020) provide more detailed descriptions of these intensity models and others used by NHC.

To mimic NHC's subjective forecast, four intensity guidance models were chosen as input to the neural network. The models are usually updated every year, so the error characteristics are not stationary.

Therefore, it is not possible to go back too far into the past for training samples. On the other hand, a reasonably large training sample is required, so the model input from at least a few years is needed. As a compromise between these two factors, the training data set includes the DSHP, LGEM, HWRF, and GFS intensity forecasts from 2013 to 2021. The CTCX and HMON models were not included, because those were not consistently available back to 2013.

To ensure time consistency across time zones, NWS data collection and forecasts are based on “synoptic” times, which are at 00, 06, 12, and 18 UTC. NHC forecasts are issued every 6 hr at 3 hr after synoptic times, so the guidance models are also run every 6 hr. However, the dynamical HWRF and GFS models are not available until after the NHC forecast is issued. To account for the delayed model guidance, the forecasts from the previous 6-hr cycle are interpolated to the current synoptic time. These are referred to as “interpolated” models and are designated as HWFI and GFSI for the HWRF and GFS, respectively. The network training includes only the interpolated models so that it is relevant to what forecasters would have available when they make their forecasts. The statistical D-SHIPS and LGEM models use input from previous forecast cycles and so are available when the forecasters are making their predictions. Although the NHC forecast is at 12-hr intervals out to 3 days and then every 24 hr thereafter, for simplicity, only the input at 24-hr intervals is considered in this study.

Again following the NHC forecast procedure, the input to the network is the deviation of each of the four input models (DSHP, LGEM, HWFI, GFSI) from the equally weighted average intensity (henceforth, termed Consensus) from these same four models. Sometimes the forecast from a particular model does not extend to 5 days. This can happen, for example, if the model forecast moves the storm over land or very cold water and the tropical cyclone dissipates. For a case to be included in the training sample at a given forecast period, at least two of the four input models must be available. The intensity forecast for the missing models is set to the average of the available models and the number of models available is provided as input to the network (NCI).

Several studies have shown that the performance of NHC’s intensity guidance models depends on the forecast situation (e.g., Bhatia and Nolan, 2015). To allow the network’s prediction of the intensity error distributions to account for this variability, several forecast-specific parameters are also included as input. These consist of the observed intensity at the start of the forecast (VMAX0), the magnitude of the storm environment 850 to 200 hPa wind shear vector (SHDC), the sea surface temperature at the tropical cyclone center (SSTN), the distance of the storm center from land (DTL), the storm latitude (SLAT), the intensity change in the 12 hr prior to the forecast initialization time (DV12), and the intensity of the Consensus (VMXC). The 12 hr prior intensity change is the same for all forecast times. All of the other parameters are averaged over the 24-hr period ending at the forecast time. All of the forecast additional parameters are obtained from the diagnostics calculated as part of the DSHP statistical-dynamical model.

NHC has forecast responsibility for all tropical cyclones in the North Atlantic (AL) and eastern North Pacific (EP) to 140 W. The NWS Central Pacific Hurricane Center (CPHC) in Honolulu has forecast responsibility for the central North Pacific (CP), which extends from 140 W to the dateline. Because the boundary between the EP and CP is not meteorologically significant, the EP and CP samples are combined. The Department of Defense Joint Typhoon Warning Center has the U.S. forecast responsibility for tropical cyclones over the rest of the globe. These tropical cyclones are not considered in this study.

The ground truth for verification of the NHC and CPHC intensity forecasts is from the “Best Track” data, which is a post-storm evaluation of all available information (Landsea and Franklin, 2013). The Best Track includes the track, maximum wind, and several other tropical cyclone parameters every 6 hr. One of the other parameters is the storm type, which sometimes includes a portion of the life cycle when tropical cyclones become extratropical cyclones. We excluded the extratropical portion of the tropical cyclones in our data set. The tropical cyclone intensity in the Best Track is almost never lower than 20 knots, so this is a lower bound on the forecast.

We task a neural network to take in the 12, single-valued predictors (see Table 1) and predict the unweighted Consensus error of the tropical cyclone intensity forecast at lead times of 24, 48, 72, 96, and

Table 1. Summary of the 12 predictors used in the model.

Predictor	Description	Units
DTL	Distance of the storm center from land	km
SHDC	Magnitude of the storm environment wind shear vector	kt
SSTN	Sea surface temperature at the tropical cyclone center	°C
SLAT	Storm latitude from the NHC official forecast	deg
DV12	Previous 12 hr intensity change	kt
VMXC	Max wind of the consensus forecast	kt
GFSI	Global Forecast System	kt
HWFI	Hurricane Weather Research and Forecast System	kt
LGEM	Logistic Growth Equation Model	kt
DSHP	Decay-Statistical Hurricane Intensity Prediction Scheme	kt
VMAX0	Observed intensity at start of forecast	kt
NCI	Number of models available	#

120 hr. The network does not output a deterministic prediction of the error, but rather, the network is designed to output a conditional probability distribution that represents a probabilistic prediction of the Consensus error. We train separate networks for the Atlantic (AL) and the East/Central Pacific (EPCP) but at time present their results in the same figure. In [Section 3](#), we will discuss the form of the probability distribution and how it is trained. In [Section 5](#), we will present the results.

3. Sinh-arcsinh-normal distribution

Here, we demonstrate the use of the sinh-arcsinh-normal (SHASH) distribution (Jones and Pewsey, 2009, 2019) to add uncertainty to neural network regression tasks. The SHASH takes four parameters in TensorFlow 2.7.0 (Abadi et al., 2015): location (μ), scale (σ), skewness (γ), and tailweight (τ) and provides a basis for representing state-dependent, heteroscedastic, and asymmetric uncertainties in an intuitive manner (Duerr et al., 2020). The SHASH may be symmetric, but it may be highly asymmetric with a weighted tail (unlike a normal distribution). The SHASH also allows for non-positive values (unlike a log-normal distribution). For our specific application, tropical cyclone intensity errors can be positive or negative, and can be skewed toward the positive tail under certain conditions. These state-dependent, heteroscedastic, and asymmetric uncertainties in the intensity error can thus be approximated as different SHASH distributions for every hurricane intensity forecast. Examples of the family of SHASH distributions are shown in [Figure 1](#), of which the normal distribution is a special case (skewness $\gamma=0$, tailweight $\tau=1$; orange curve in [Figure 1b](#)). A detailed description of the SHASH formulation and implementation is provided in [Appendix B](#).

The neural network is tasked with predicting the four parameters of the SHASH distribution ([Figure 1a](#)). That is, the output of the network contains four units capturing μ , σ , γ , and τ . The parameters σ (scale) and τ (tailweight) must be strictly positive. To accomplish this, we follow a common trick in computer science (Duerr et al., 2020) to ensure that σ and τ are always strictly positive by tasking the network to predict the $\log(\sigma)$ and the $\log(\tau)$ rather than σ and τ themselves. Here, we predict the four parameters of the SHASH distribution using fully connected neural networks. However, a benefit of this general approach for including uncertainty is that it can be easily applied to most any neural network architecture, as it only requires modification of the output layer and the loss function (see [Section 3.1](#)).

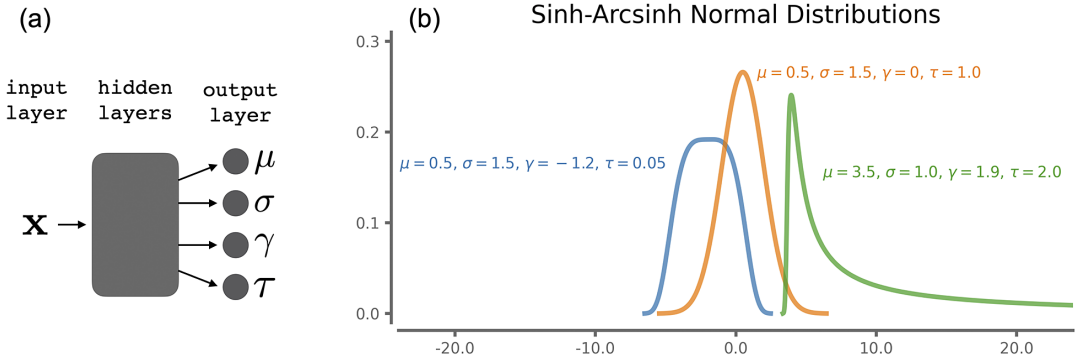


Figure 1. (a) Neural network architecture and (b) example sinh-arcsinh-normal (SHASH) distributions for combinations of parameters.

3.1. The loss function

The neural network architecture shown in Figure 1a trains using the negative log-likelihood loss defined for the i th input sample, x_i , as

$$\mathcal{L}(x_i) = -\log p_i. \tag{1}$$

where p_i is the value of the SHASH probability density function, \mathcal{P} , with predicted parameters $(\mu, \sigma, \gamma, \tau)$ evaluated at the true label y_i . That is,

$$p_i = \mathcal{P}(y_i | \mu, \sigma, \gamma, \tau). \tag{2}$$

Figure 2 shows schematically how the probability p_i depends on the specific parameters of the distribution predicted by the network. For example, if the predicted distribution is overconfident (the distribution’s width is too small), p_i will be small and the loss \mathcal{L} will be large (Figure 2a). If the network is underconfident (the distribution’s width is too large), p_i will also be small and the loss \mathcal{L} will once again be large (Figure 2b). Like Goldilocks, the network needs to get things “just right,” by properly estimating its uncertainty to obtain its best guess. Better predictions are associated with larger p_i , and thus smaller loss \mathcal{L} (Figure 2c). Note that this approach is directly tied to the standard method of parameter estimation in statistics known as *maximum likelihood estimation* (Duerr et al., 2020).

While this work highlights the sinh-arcsinh-normal probability density function, the loss function in Eq. (1) can be used for any well-behaved probability distribution. The trick to training the neural network is that the loss for observation i is the predicted probability density function evaluated at the observed y_i . For example, if the y variable denotes a percentage or proportion, then a distribution with finite support from 0 to 1 may be more appropriate. The beta and Kumaraswamy are two such distributions that have been used to model hydrological variables such as daily rainfall (e.g., Mielke, 1975; Kumaraswamy, 1980). Even so, we believe that the SHASH offers a versatile, intuitive family of distributions that will likely be applicable to a wide range of earth science applications.

3.2. Network architecture and training specifics

For all SHASH prediction tasks, we train a fully connected neural network (abbreviated throughout as NN) with two hidden layers of 15 and 10 units, respectively, to predict the first three parameters of the SHASH distribution (i.e., μ, σ, γ). We found that including the tailweight τ did not improve the network performance, and so we set $\tau = 1.0$ throughout. The rectified linear activation function (ReLU) is used in all hidden layers. We train the network with the negative log-likelihood loss given in Eq. (1) using the Adam optimizer in TensorFlow with a learning rate of 0.0001 and batch size of 64. The network is trained to minimize the loss on the training data, and training is halted using early stopping when the validation loss has not decreased for 250 epochs. When this occurs, the network returns the network weights associated with the best validation loss.

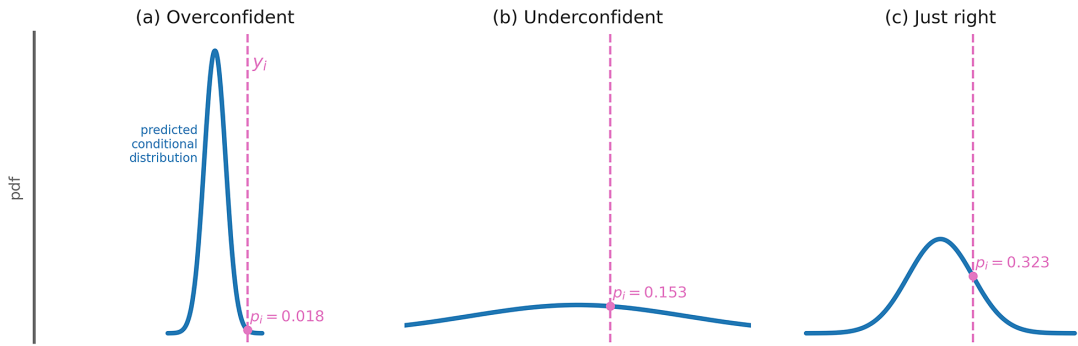


Figure 2. Schematic showing how the loss function probability p_i is dependent on the predicted probability distribution.

The data is split into training, validation, and testing sets. To explore the sensitivity of the results to the random training/validation split as well as the randomly initialized weights, each network setup is trained five different times using five different random seeds. Testing results are then shown for the network with the lowest validation error of the five. In addition, we train five different networks for each possible nine testing years (from 2013 to 2021). Figures 3–5 show case studies and results for one specific network using a random seed of 739 for testing year 2020 to provide readers with specific examples. In this case, the testing set is composed of all 2020 tropical cyclone forecasts, and the validation set is chosen as a random 200 samples from those not included in the testing set. The rest of the samples are then reserved for training. Each forecast lead time has a different number of samples available, but for a lead time of 48 hr, this results in 1,961 training samples, 200 validation samples, and 124 testing samples for the Eastern/Central Pacific. The number of samples for all lead and basin combinations for testing year 2020 is provided in Appendix A.

4. Alternative uncertainty approaches

4.1. Bayesian neural network

The published research on Bayesian Neural Networks is immense and growing (e.g., Jospin et al., 2022). Our comparison here is based on vanilla Bayesian Neural Networks for regression as discussed in Duerr et al. (2020) and implemented in TensorFlow 2.7.0. This approach uses Bayes by backprop with Gaussian priors, as defined in Blundell et al. (2015), a variational inference approximation, as presented in Graves (2011) (which is built upon the work of Hinton and Camp, 1993), and computations using the TensorFlow DenseFlipout layers, which are based on Wen et al. (2018).

The BNN architecture and training setup is similar to that of the SHASH approach described in Section 3.2, except it directly draws samples from the posterior predictive distribution of the hurricane intensity errors. In addition, the BNN uses a DenseFlipout layer class to include probabilistic weights and biases that take the form of Gaussian distributions. Otherwise, all other hyperparameters and training approaches remain the same. Unlike the SHASH, however, at inference, the BNN only outputs a single prediction of the Consensus error per one forward pass of a given sample. Thus, to create a BNN-predicted distribution we push each sample through the BNN 5,000 times to create a predicted conditional distribution comparable to the SHASH.

4.2. Monte Carlo Dropout

We additionally present Monte Carlo Dropout (MC Dropout) as a second alternative uncertainty quantification method for comparison. Srivastava et al. (2014) introduced Dropout as a method for reducing the chance of overfitting in neural networks. Specifically, during training, a specific percentage

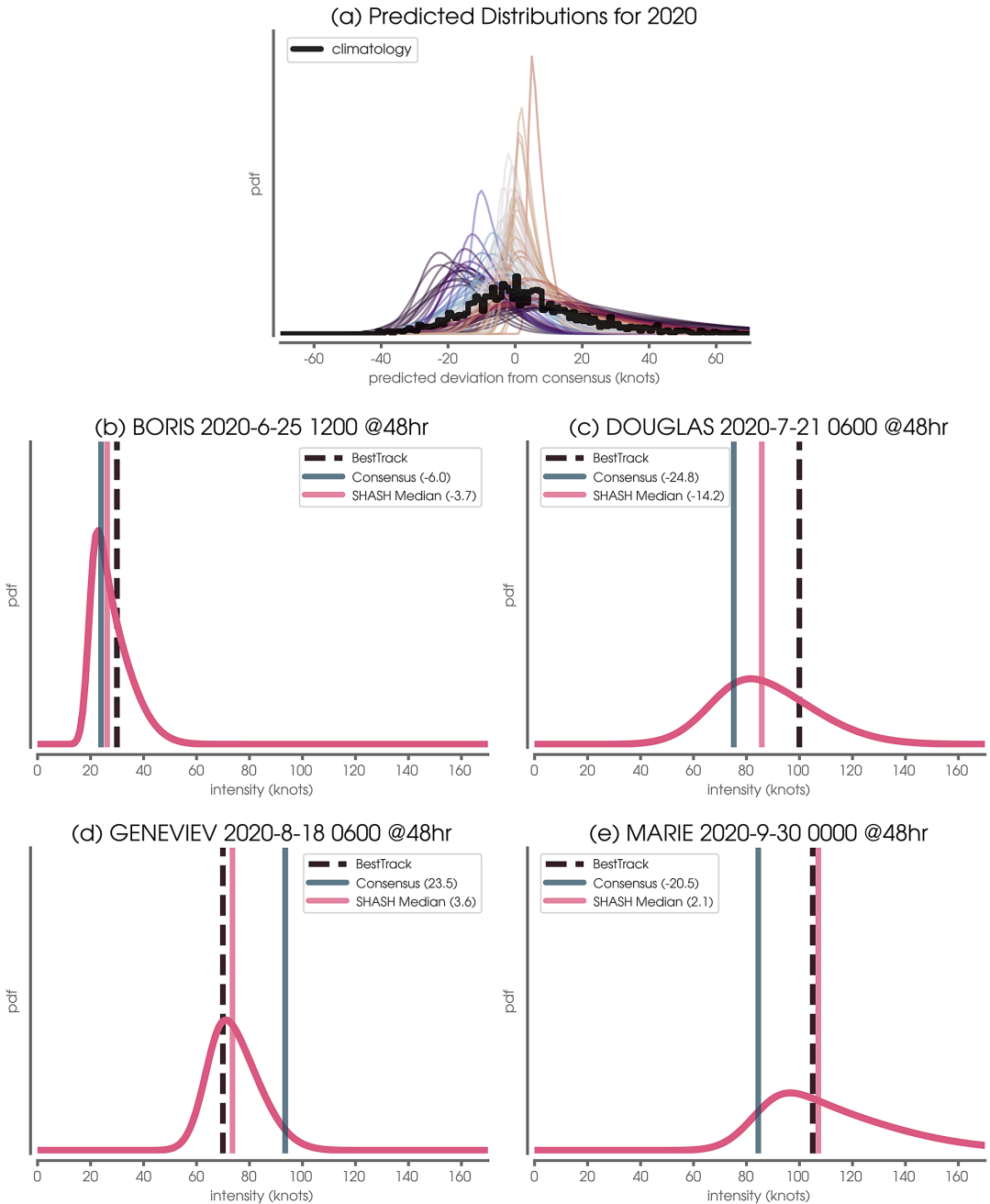


Figure 3. (a) Predicted distributions for testing year 2020. The thick black line denotes the climatological Consensus error distribution across all training and validation samples. (b–e) The example predicted conditional distributions using the SHASH architecture as well as the Best Track verification Consensus forecast. This example is for the Eastern/Central Pacific at 48 hr lead time.

of each layer’s units are temporarily removed (“dropped out”) so that the network must learn to spread predictive information across nodes to make accurate predictions. Dropout is typically only used during training and then turned off during inference. However, it has recently gained traction as a method for uncertainty quantification when left on during inference as well (Gal and Ghahramani, 2015). That is, the

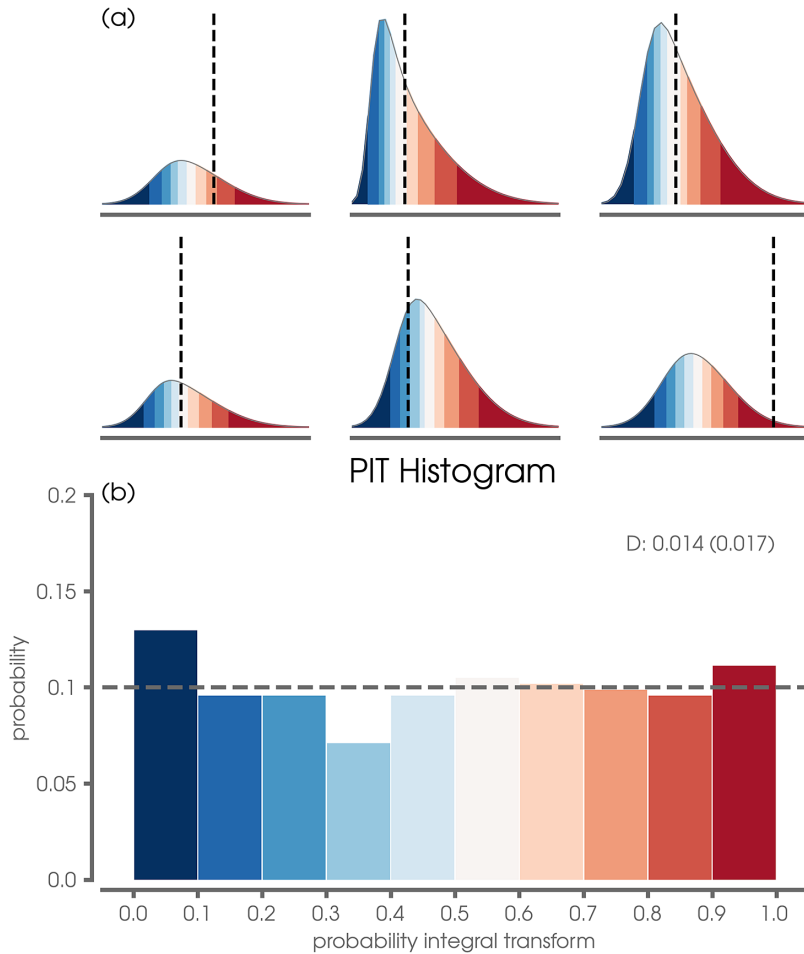


Figure 4. (a) Six example predictions to demonstrate the probability integral transform (PIT) calculation where colored shading denotes different percentile bins in increments of 10%. (b) Final PIT histogram computed for the validation and testing data for the network trained with 2020 as the leave-one-out year. The calibration deviation statistic, D , is printed in gray; the expected calibration deviation for a perfectly calibrated forecast is given in parentheses. These examples are for the Eastern/Central Pacific at 48 hr lead time.

MC Dropout method leaves Dropout during inference to obtain a range of predictions for a given sample depending on which units are randomly dropped out.

The MC Dropout architecture and training setup is similar to that of the SHASH approach described in Section 3.2, except (like the BNN) it directly draws samples from the posterior predictive distribution of the hurricane intensity errors. There are additional important differences between the MC Dropout setup and the SHASH and BNN approaches. First, we use a mean absolute error loss function. Next, we train the NN with a dropout rate of 75% in all hidden layers. To that end, we increase the number of units in each layer to have 60 units in the first year and 40 units in the second layer. We note that keeping the number of units the same as in the SHASH and BNN models (i.e., 15 units and 10 units in each layer, respectively) and using a dropout rate of 25% yielded similar conclusions although the MC Dropout model performed more poorly than the architecture presented here (not shown). Finally, we found that a smaller learning rate of 0.00005 was required to train the MC Dropout model. As is the case for the BNN approaches, at

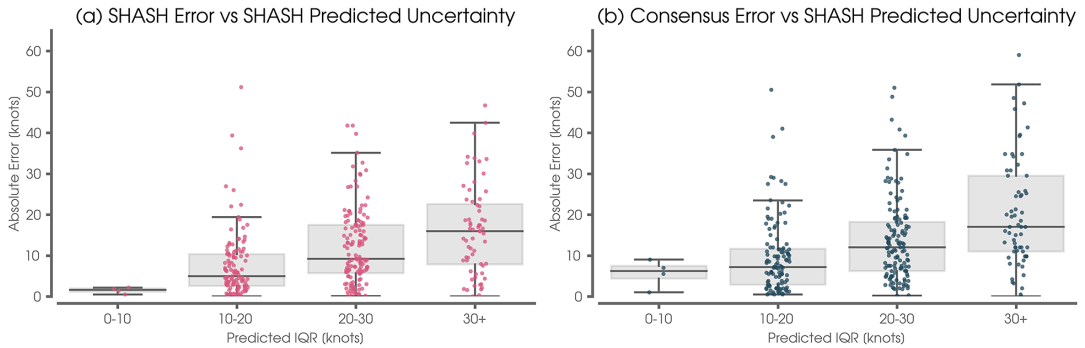


Figure 5. (a) Neural network (NN) mean absolute error versus the network predicted inter-quartile range (IQR). The error is defined as the median of the predicted SHASH distribution minus the Best Track verification. (b) As in (a), but for the Consensus error vs the network-predicted IQR. For both panels, the statistics are computed over the validation and training sets to increase the sample size. This example is for the Eastern/Central Pacific at 48 hr lead time.

inference the MC Dropout approach only outputs a single prediction of the Consensus error per one forward pass of a given sample. Thus, we create an MC Dropout-predicted conditional distribution for each sample by pushing each sample through the network 5,000 times to create a predicted conditional distribution comparable to the SHASH and BNN.

5. Results

We first examine the neural network SHASH predictions for estimating the Consensus error for tropical cyclone intensities over the Eastern/Central Pacific at 48-hr lead times. After discussing a few specific forecasts, we then present multiple evaluation metrics to demonstrate the utility of the SHASH approach. We then end the section with a comparison between the SHASH and two other neural network uncertainty approaches.

5.1. Uncertainty estimation with the SHASH

All predicted SHASH conditional distributions for the Eastern/Central Pacific at a 48-hr lead time and testing year 2020 are plotted in Figure 3a, where the climatological Consensus error distribution of all other years (i.e., training and validation) is shown in black. Although the climatological errors of the Consensus are relatively symmetric about zero, the network predicts a wide range of SHASH distributions. This includes varying location, spread, and skewness depending on the specific 2020 forecast sample. Because the neural network is tasked to predict the Consensus error rather than the intensity itself, negative values denote that the network predicts the Consensus intensity to be too large, and positive values denote that the network predicts the Consensus intensity to be too small.

Four example testing forecast samples are shown in Figure 3b–e. The network’s predicted distribution is plotted in pink, where the Consensus prediction has been added to the predicted SHASH distribution to convert the SHASH to units of tropical cyclone intensity (rather than Consensus intensity error). The vertical dashed line denotes the Best Track verification (i.e., the intensity that actually occurred) and the vertical blue line denotes the Consensus prediction. As already discussed, the network predicts a range of SHASH distributions depending on the specific forecast. For example, the predicted SHASH is heavily positively skewed, but relatively narrow for BORIS (Figure 3b) suggesting that the network is relatively confident in its prediction. The fact that the network places a near-zero probability that BORIS’ intensity will drop below 20 knots is evidence that the network has learned that tropical depressions rarely exhibit intensities less than this, as mentioned in Section 2. In contrast, the network is far less confident in

MARIE's intensity (Figure 3e); subsequently, and so the predicted SHASH exhibits a much wider distribution with a longer positive tail.

A benefit of tasking the network to make a probabilistic forecast is that from this we can produce a range of probabilistic statements about the future tropical cyclone intensity. However, it can at times be helpful to produce a deterministic prediction as well. Here we use the median of the SHASH (shown as a vertical pink line in Figure 3b–e). For all four examples shown here, the median of the SHASH prediction (vertical pink line) is closer to the Best Track verification (vertical dashed line) than the Consensus (vertical blue line), demonstrating that the SHASH can improve the intensity forecast in a deterministic sense and provide a quantification of uncertainty. We present summary metrics of this improvement in the next subsection.

5.2. Evaluation metrics

After training the network, what evidence do we have that our model is any good? On the one hand, one could just compare the true y value with a deterministic value (i.e., the mean or median of the predicted conditional distribution). However, this type of residual diagnostic does not address whether the predicted uncertainties are useful. While many metrics for evaluating probabilistic predictions exist (e.g., Garg et al., 2022), here we discuss three.

The first metric is the simplest. It quantifies the fraction of samples where the true intensity error y falls between the 25th and 75th percentiles of the predicted SHASH distributions. We call this fraction the “IQR capture fraction.” If the network produces reliable forecasts, then y should fall within the IQR interval half of the time and the IQR capture fraction should be approximately 0.5. For our SHASH predictions of Eastern/Central Pacific tropical cyclone intensity errors at a 48-hr lead time and 2020 testing year (Figure 6d), the IQR capture fraction is 0.48 over the validation and testing sets (we include validation to increase the sample size for this statistic).

The IQR capture fraction quantifies the fit of predictions that fall in the middle, but what about other percentile combinations? Or the tails of the distribution? Dawid (1984) introduced the probability integral transform (PIT) as a calibration check for probabilistic forecasts. The PIT works similarly to the IQR capture fraction but is more general. Consider sample i . Our trained neural network gives us a conditional probability distribution for y as a function of x_i . If we denote the cumulative distribution function (CDF) for this conditional distribution $F(y|x_i)$ then the probability integral transform (PIT) value for sample i , which we denote p_i , is

$$p_i = F(y_i|x_i). \quad (3)$$

As explained in Gneiting and Katzfuss (2014), p_i is the predicted CDF evaluated during the observation. Six such example calculations of p_i are shown in Figure 4a. The histogram of all such values over the data set is called the PIT histogram (Figure 4b). If the predictive model is ideal, then the PIT histogram follows a uniform distribution (Gneiting et al., 2007).

Figure 4b shows the PIT histogram for the validation and testing samples for the Eastern/Central Pacific predictions at a 48-hr lead time for testing year 2020. The validation data are included to increase sample size, since the PIT histogram becomes meaningless when the evaluation set is too small (Hamill, 2001; Bourdin et al., 2014). A perfectly calibrated forecast is expected to have a PIT histogram that is uniform distribution (that is flat). As seen in Figure 4b, the predicted PIT histogram is nearly uniform. Following Nipen and Stull (2011) and Bourdin et al. (2014), we compute the PIT D statistic to quantify the degree of deviation from a flat PIT histogram:

$$D = \sqrt{\frac{1}{B} \sum_{k=1}^B \left(b_k - \frac{1}{B} \right)^2}, \quad (4)$$

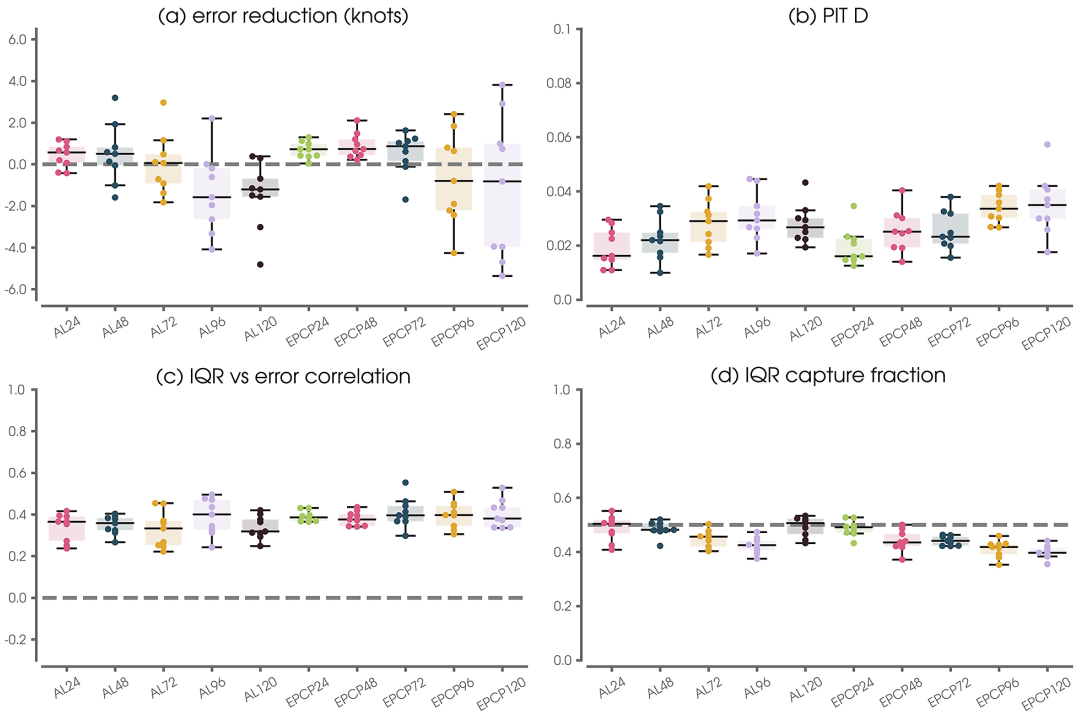


Figure 6. SHASH performance metrics across a range of basins and lead times for each of the nine leave-one-out testing years (denoted by dots). The x-axis label convention is such that AL denotes the Atlantic basin and EPCP denotes the combined Eastern and Central Pacific basins. Numbers denote the forecast lead time in hours. Panel (a) shows testing results only, while panels (b)–(d) show results over validation and testing sets to increase the sample size for the computed statistics. See the text for details on the calculation of each metric.

where k is an integer denoting the bin number that ranges from 1 to the total number of bins B and b_k denotes the bin frequency of the k th bin. For our case, $B = 10$ and $D = 0.014$. Again following Bourdin et al. (2014), a perfectly calibrated forecast will produce a PIT histogram that is perfectly flat. The expected deviation is given by

$$E[D_p] = \sqrt{\frac{1 - B^{-1}}{TB}}, \tag{5}$$

where D_p denotes the PIT D statistic for a perfectly calibrated forecast and T is the total number of samples over which the PIT was computed. For our case, this expected deviation is $E[D_p] = 0.017$. The computed D for the PIT histogram shown in Figure 4b is $D = 0.014$, and so, it cannot be distinguished from that produced by a perfectly calibrated forecast. We will make use of the PIT D statistics to summarize the calibration of all networks later in this section.

An additional way to visualize the utility of the network’s probabilistic forecast is to assess the extent to which a wider predicted SHASH relates to larger errors using the median as a deterministic prediction. Put another way, when the SHASH distribution is narrow, we would like the median of the predicted SHASH to be closer to the truth than when the SHASH distribution is wide. We quantify the width of the SHASH using the interquartile range (IQR) and plot the NN’s deterministic error against this predicted IQR in Figure 5a. Indeed, we see a strong correlation between the network’s deterministic error and the IQR of the predicted SHASH, demonstrating that the width of the predicted distribution can be used as a measure of uncertainty. Furthermore, Figure 5b shows that the IQR of the predicted SHASH also correlates with the

Consensus prediction error. That is, the width of the predicted SHASH can be used as a metric to assess uncertainty in the Consensus forecast itself.

Equipped with multiple metrics to evaluate the NN's SHASH prediction, Figure 6 summarizes the deterministic errors (Figure 6a) and the three probabilistic metrics (Figure 6b–d) across all nine leave-one-out testing years for a range of lead times and ocean basins (x -axis). Our results show that the deterministic NN forecast (based on the median of the predicted SHASH) can improve upon the Consensus forecast at shorter lead times in both basins, but struggles to improve upon the Consensus at 96- and 120-hr lead times (Figure 6a).

Even in the event that the NN does not improve upon the Consensus forecast in a deterministic sense, Figure 6b–d demonstrates that the SHASH predictions provide useful uncertainty quantifications. The PIT D statistics show small values (Figure 6b) and the IQR capture fractions fall near 0.5 (Figure 6d). Figure 6c summarizes results of the comparison shown in Figure 5a by displaying the Spearman rank correlation between the NN absolute error (based on the median) and the predicted IQR. For context, the example shown in Figure 5a exhibits a Spearman correlation of 0.5. Thus, we see that for all combinations of lead time and basin, the NN-SHASH provides a meaningful measure of uncertainty that correlates with the deterministic error.

5.2. SHASH applications to rapid intensification probabilities

Although NHC's intensity forecast skill has shown significant improvement over the last decade (Cangialosi et al., 2020), there has been less progress in the ability forecast rapid intensification (RI) (DeMaria et al., 2021). As described by Kaplan (2015), there are a number of definitions of RI, but the most common ones are intensity increases of 30 knots or greater in 24 hr, 55 knots or greater in 48 hr, and 65 knots in 72 hr. As shown by DeMaria et al. (2021), dynamical models such as HWRF and HMON have shown some ability to forecast RI in the past few years. However, the most accurate guidance is based on statistical methods such as linear discriminate analysis or logistic regression, where RI is treated as a classification problem.

Because the NN-SHASH provides complete error distribution, it can be used to provide RI guidance. We further demonstrate the benefits of the NN-SHASH approach by using the predicted conditional SHASH distribution to quantify the probability of tropical cyclone rapid intensification (RI). Here, we use the predicted SHASH to forecast the probability of RI occurrence. An example of this is shown in Figure 7a for the Atlantic 48-hr forecast for Hurricane Michael on October 10, 2018. The intensity at the time of forecast (50 knots) is shown by the vertical gray line and the predicted intensity distribution at 48 hr is denoted by the pink curve. By definition, RI requires an increase of 55 knots over a 48-hr period, which corresponds to an intensity of $50 + 55 = 105$ knots. Thus, by integrating under the predicted SHASH distribution from 105 knots and above, we obtain a predicted probability of RI of 47%. In fact, Michael did undergo RI during this time, increasing its intensity over 48 hr by 60 knots to 110 knots (dashed black line).

We compute the probability of RI over all predictions for the Atlantic and Eastern/Central Pacific for all nine leave-one-out testing years and group the results by whether or not RI actually occurred (Figure 7b). For nearly all cases that undergo RI (pink boxes), the NN predicts a non-zero probability of RI. Contrast this with cases that do not undergo RI (gray boxes), where nearly all cases exhibit a near-zero predicted probability. The Mann–Whitney U statistic comparing the distributions in each panel of Figure 7 result in p -values of $2e - 194$, $4e - 117$, and $3e - 80$ for the three panels in Figure 7b, respectively. Thus, the NN approach is clearly able to distinguish between cases that will likely undergo RI and those that will not. The precision-recall curves shown in Figure 7c further demonstrate that the NN has skill in predicting RI at all three lead times. While a more thorough analysis is required to quantify the extent to which our RI predictions improve upon current operational methods, our focus here is to demonstrate the potential utility of the approach.

Taking our analysis one step further, we utilize AI explainability methods (e.g., McGovern et al., 2019; Mamalakis et al., 2022) to better understand why the NN predicted the distribution that it did.

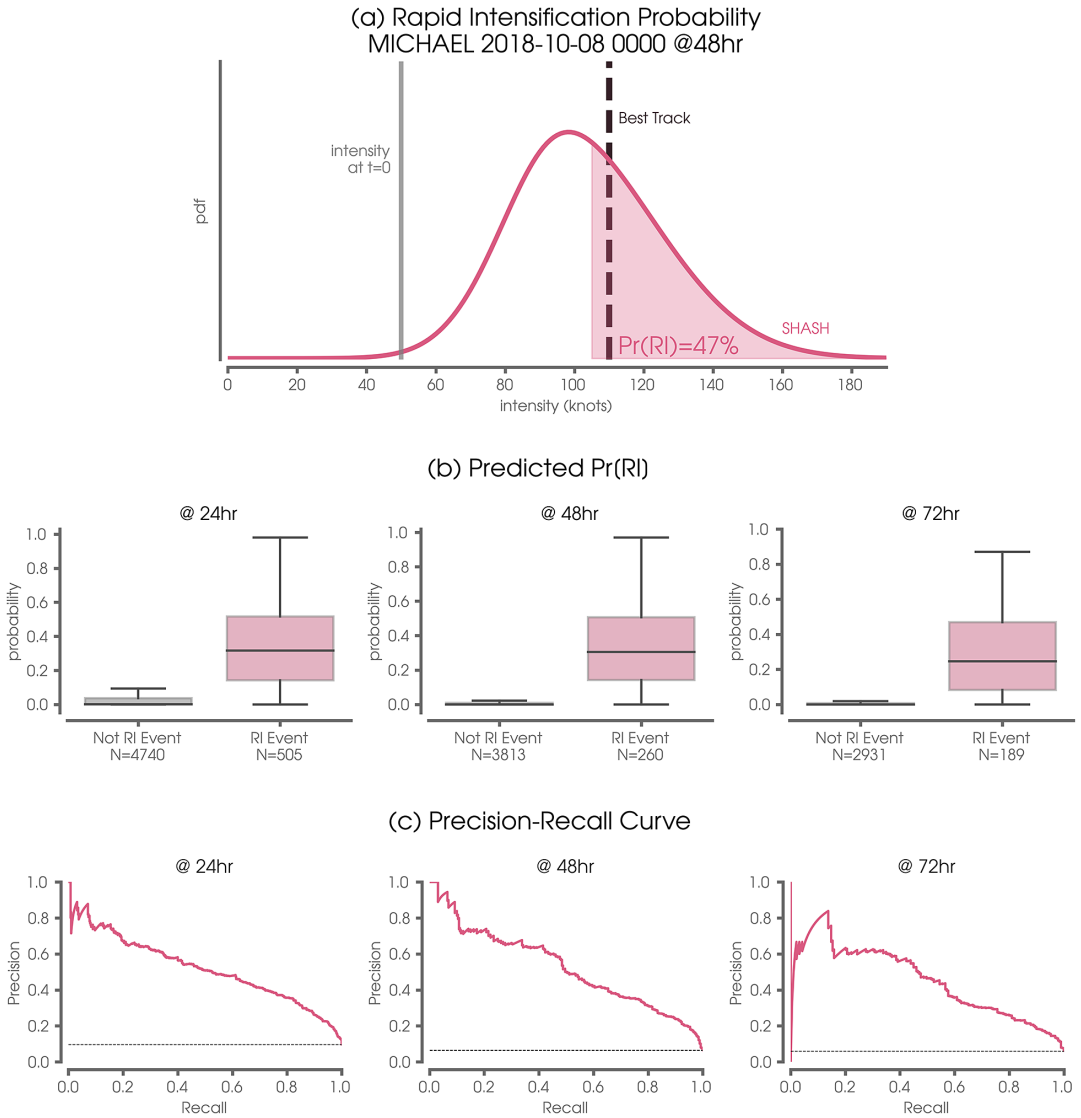


Figure 7. (a) Example case study demonstrating the utility of the SHASH for predicting the probability of rapid intensification ($Pr(RI)$); pink shading). The pink curve denotes the predicted conditional distribution by the SHASH at 48-hr lead time for Hurricane Michael on October 8, 2018. The gray vertical line denotes the storm intensity at the time of the forecast and the vertical dashed line denotes the Best Track verification. (b) Predicted probability of rapid intensification at various lead times for all East/Central Pacific and Atlantic storms for all nine leave-one-out testing years. The gray box plot denotes predicted probabilities for storms that did not undergo rapid intensification, while the pink box plot denotes predicted probabilities for storms that did. (c) As in (b), but the precision-recall curves for RI as a function of lead time. The dashed black line denotes the baseline precision in the case of no skill.

For example, we can further explore the high predicted probability of RI by plotting the gradient of the output with respect to the input features of the NN for the 48-hr prediction of Michael on October 10, 2018. Since the gradient is computed for each output separately, we obtain a measure of the sensitivity of the predicted SHASH parameters to small increases in each of the 12 features (Figure 8a). Based on this gradient calculation, the NN would have predicted smaller parameters if the storm had been slightly

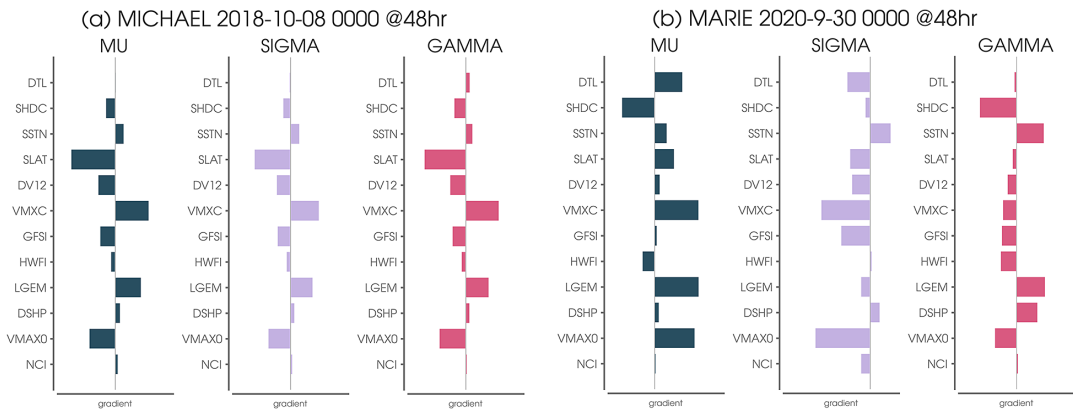


Figure 8. (a) Neural network gradient for the 48-hr SHASH prediction for Hurricane Michael on October 8, 2018. The gradient describes how small increases in each input predictor would have changed the prediction of each of the three SHASH parameters (the tailweight τ is fixed to 1.0). (b) As in (a), but for Hurricane Marie on September 30, 2020.

further north (i.e., more positive SLAT). Furthermore, had the Consensus (VMXC) been slightly larger, the NN would also have predicted larger SHASH parameters. Interestingly, the NN appears more sensitive to the LGEM forecast than the others for this particular prediction, suggesting that had the LGEM forecast been larger the NN would have increased its predicted parameters as well. We repeated this analysis for Hurricane Marie for the same case shown in Figure 3e, and the results are plotted in Figure 8b. Unlike for Hurricane Michael, had the Consensus (VMXC) been slightly larger, the NN would have predicted larger μ but smaller σ . Furthermore, had the intensity at the time of forecast (VMAX0) been slightly larger, the NN would have also increased its μ and decreased σ . This suggests that explainability methods can be used to understand differences in the NN’s decision-making process for specific forecasts. We leave the exploration of additional case studies and explainability methods for future work.

5.3. Comparison with alternative neural network uncertainty approaches

It is worth briefly contrasting the SHASH approach discussed here with that of other approaches such as Monte Carlo Dropout (MC Dropout) and Bayesian neural networks (BNN) that have become go-to methods for incorporating uncertainty into artificial neural networks (e.g., Wilson, 2020; Foster et al., 2021). While both MC Dropout and BNN architectures can vary greatly in detail, we focus here on a simple implementation of each. Our aim is not to provide an exhaustive comparison, nor to claim that one method is the “winner” over the others but, rather, to provide a comparison between the methods using the same problem setup and data. Furthermore, our aim is not to review, compare, or summarize the hundreds (perhaps thousands) of species and subspecies of uncertainty quantification present in the machine learning ecosystem (see, e.g., Abdar et al., 2021; Jospin et al., 2022). Instead, we implement BNNs and MC Dropout using the default configurations provided by TensorFlow 2.7.0 (<https://www.tensorflow.org/>) and its TensorFlow Probability 0.15.0 package (<https://www.tensorflow.org/probability>) as a scientist might when trying to determine which method to explore further.

Predictions for the four use cases discussed in Section 5.2 are shown in Figure 9, but now compare the three uncertainty quantification approaches (see Section 4 for details; SHASH predictions are identical to those in Figure 2b–d). While all three approaches produce predicted conditional distributions, MC Dropout tends to produce distributions that are much narrower than the other two methods and the BNN-predicted distributions tend to be more symmetric. This is particularly evident for BORIS (Figure 9a), where the BNN predicts non-zero probabilities of 0 knot intensities.

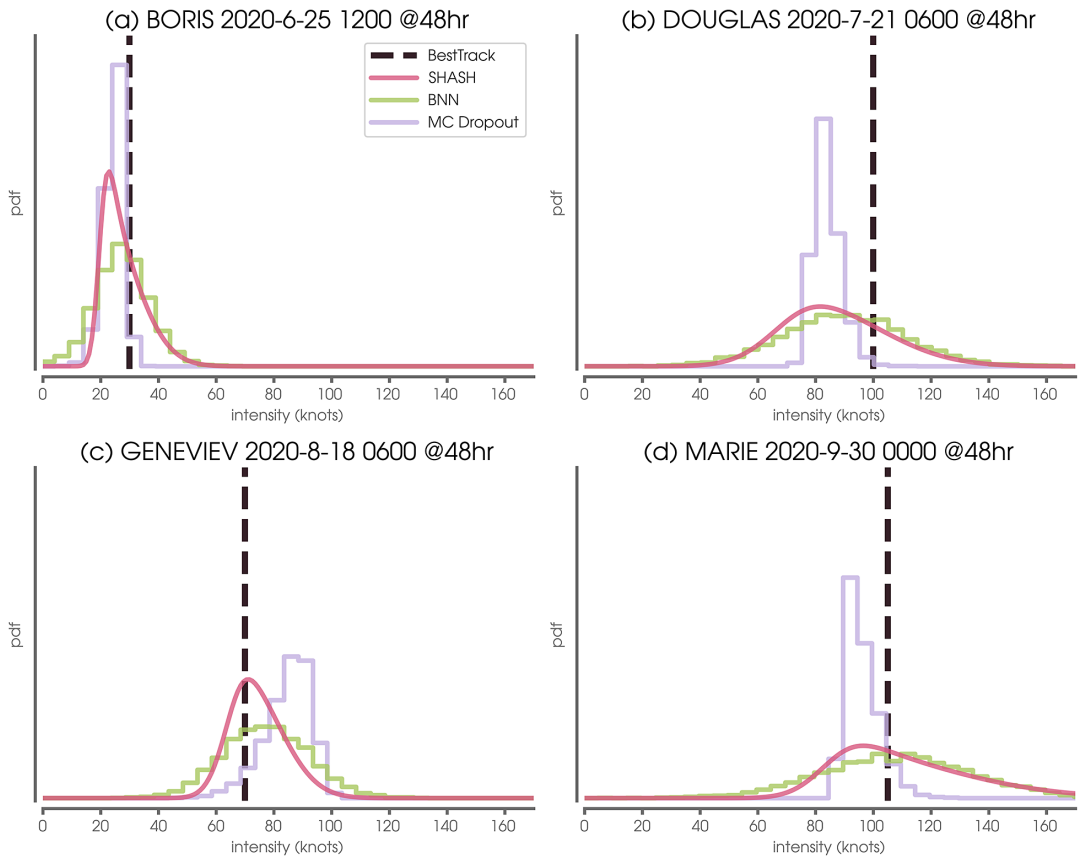


Figure 9. Example conditional distributions predicted by four neural network probabilistic methods. Vertical dashed line denotes the Best Track verification.

Figure 10 shows summary metrics across all nine leave-one-out testing years as in Figure 6 but compare the three different approaches for estimating uncertainty. While all three approaches are similarly able to reduce the Consensus prediction error in a deterministic sense, panels (b)–(d) show that their probabilistic properties differ. MC Dropout tends to produce distributions that are much too narrow. This is quantified by the large PIT D statistics (Figure 10b), a lack of strong correlation between the IQR and deterministic error (Figure 10c), and IQR capture fractions far below 0.5 (Figure 10d). This failure of MC Dropout was also noted by Garg et al. (2022) for medium-range weather forecasts. The BNN performs much more similar to the simple SHASH, and in some cases may even perform better, although only marginally so. Trade-offs between the SHASH and BNN approaches will be discussed further in Section 6.

6. Discussion

Here, we present a simple method that estimates the conditional distribution for each sample. It was originally proposed by Nix and Weigend (1994) and has been presented as a standard approach in recent literature, for example, Duerr et al. (2020), the TensorFlow manual, and many data science blogs. Even so, it appears relatively unknown in the earth science community. The approach is simple, can be applied to most any network architecture, and can be adapted to different uncertainty distributions via the choice of the underlying distribution. Here, we explore the family of sinh-arcsinh-normal (SHASH) distributions (Jones and Pewsey, 2009) as a general set that can capture location, spread, and skewness of the posterior

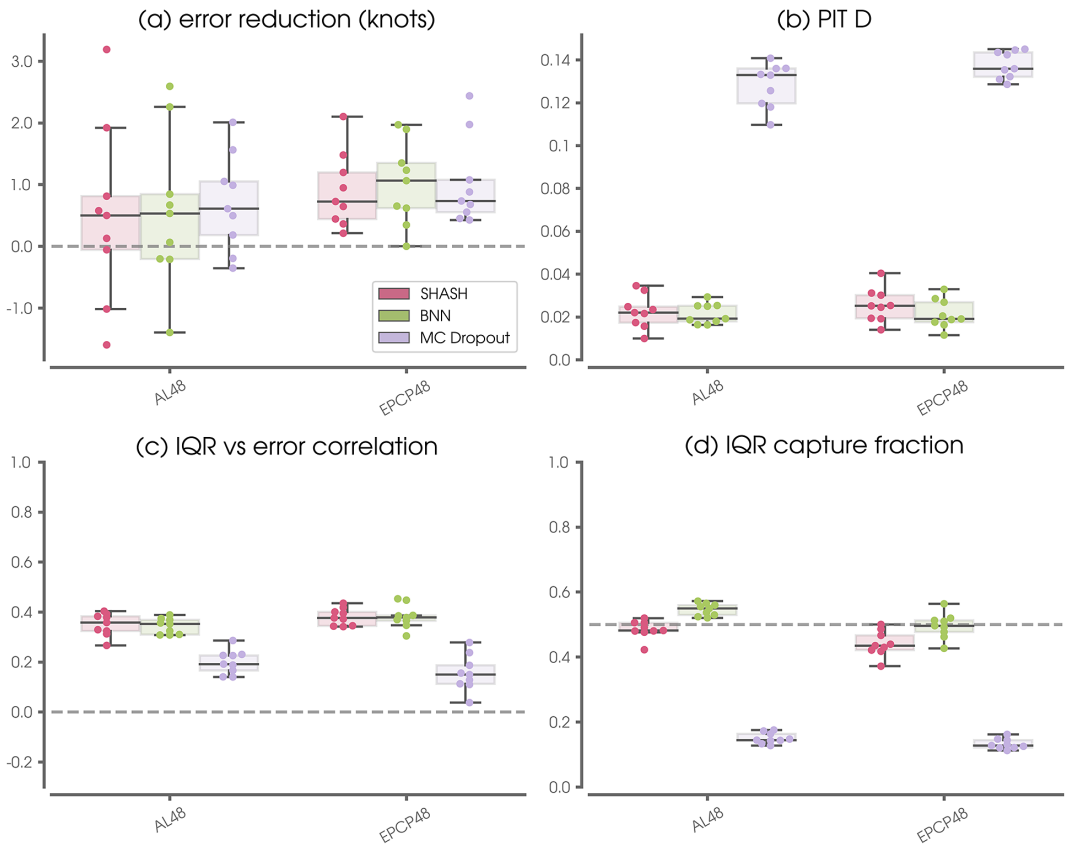


Figure 10. As in Figure 6, but for the SHASH, BNN, and MC-Dropout approaches for Atlantic (AL) and Pacific (EPCP) forecasts at 48-hr lead times for all nine leave-one-out testing years.

distribution in an intuitive manner. However, we note that other distributions (e.g., the lognormal distribution) may be better choices for specific applications.

In addition to being straightforward to understand and implement, the NN-SHASH approach is computationally efficient, especially at inference. For example, on a late 2019 iMac with six cores and 32 GB of RAM, the NN-SHASH took 5 s to predict distributions for 124 testing samples. In contrast, MC Dropout took 9 s to predict the distributions using 5,000 draws each, and the BNN took 163 s to predict the distributions using 5,000 draws each. Thus, although the BNN performs similarly to the NN-SHASH, it is more computationally expensive at inference and significantly more difficult to understand given the complexities of the variational inference method employed during training.

Our SHASH approach aims to quantify the predictive uncertainty, being agnostic to whether the uncertainty comes from the data noise or from the model itself. The SHASH model presented here uses a maximum likelihood approach to estimate the parameters of the SHASH distribution, and does not explicitly quantify, or account for, errors in the learned SHASH parameters. Thus, the proposed approach does not account for errors in the learned parameters (and could underestimate the true predictive uncertainty) when either the SHASH distribution provides a poor approximation to the true predictive distribution or when the SHASH parameter estimates are inaccurate. For example, this may occur when there is too little training data in the neighborhood of the input. With that said, our leave-one-out (year by year) analysis captures uncertainties in the learned SHASH parameters via training nine separate networks (see Figures 6 and 10).

Finally, we note that while TensorFlow provides an implementation of the family of sinh-arcsinh distributions, it does not provide certain SHASH metrics (e.g., mean, standard deviation, and variance) at the time of publication of this work. We have provided documentation in [Appendix B](#) of how we have implemented these metrics for the sinh-arcsinh-normal distribution. We also provide code to fill this gap.

7. Conclusions

Estimating the parameters of a sinh-arcsinh-normal probability distribution function is a simple, straightforward method for adding uncertainty to neural network regression tasks. The method provides reliable uncertainty estimates when applied to predictions of tropical cyclone intensity errors. The authors believe it will become a powerful, go-to method moving forward.

Author contribution. Conceptualization: E.A.B., R.J.B., M.D.; Data curation: M.D.; Data visualisation: E.A.B.; Methodology: E.A.B., R.J.B.; Writing—original draft: E.A.B., R.J.B., M.D. All authors approved the final submitted draft.

Competing interest. The authors declare none.

Data availability statement. Atlantic, eastern North Pacific, and central North Pacific operational model and best track data were obtained from the National Hurricane Center. The code and data set prepared for this work can be found on Zenodo at the following permanent DOI: <https://doi.org/10.5281/zenodo.7915589>.

Ethics statement. The research meets all ethical guidelines, including adherence to the legal requirements of the study country.

Funding statement. This research was supported, in part, by a National Science Foundation CAREER Award AGS-1749261 and the National Science Foundation AI Institute for Research on Trustworthy AI in Weather, Climate, and Coastal Oceanography (AI2ES) under NSF grant ICER-2019758.

References

- Agarwal A, Barham P, Brevdo E, Chen Z, Citro C, Corrado GS, Davis A, Dean J, Devin M, Ghemawat S, Goodfellow I, Harp A, Irving G, Isard M, Jozefowicz R, Jia Y, Kaiser L, Kudlur M, Levenberg J, Mané D, Schuster M, Monga R, Moore S, Murray D, Olah C, Shlens J, Steiner B, Sutskever I, Talwar K, Tucker P, Vanhoucke V, Vasudevan V, Viégas F, Vinyals O, Warden P, Wattenberg M, Wicke M, Yu Y and Zheng X. (2015) TensorFlow: Large-scale machine learning on heterogeneous systems. Available at <https://www.tensorflow.org/>.
- Abdar M, Pourpanah F, Hussain S, Rezazadegan D, Liu L, Ghavamzadeh M, Fieguth P, Cao X, Khosravi A, Acharya UR, Makarek V and Nahavandi S (2021) A review of uncertainty quantification in deep learning: Techniques, applications and challenges. *Information Fusion* 76, 243–297. <https://doi.org/10.1016/j.inffus.2021.05.008>
- Amini A, Schwarting W, Soleimany A and Rus D (2019) Deep evidential regression. [arXiv:1910.02600](https://arxiv.org/abs/1910.02600).
- Barnes EA and Barnes RJ (2021) Controlled abstention neural networks for identifying skillful predictions for regression problems. *Journal of Advances in Modeling Earth Systems* 13(12). <https://doi.org/10.1029/2021ms002575>
- Bhatia KT and Nolan DS (2015) Prediction of intensity model error (PRIME) for Atlantic basin tropical cyclones. *Weather and Forecasting* 30(6), 1845–1865. <https://doi.org/10.1175/WAF-D-15-0064.1>
- Blundell C, Cornebise J, Kavukcuoglu K and Wierstra D (2015) Weight uncertainty in neural networks. <https://doi.org/10.48550/ARXIV.1505.05424>
- Bourdin DR, Nipen TN and Stull RB (2014) Reliable probabilistic forecasts from an ensemble reservoir inflow forecasting system. *Water Resources Research* 50(4), 3108–3130. <https://doi.org/10.1002/2014wr015462>
- Cangialosi JP (2022) National Hurricane Center Forecast Verification Report - 2021 Hurricane Season. Tech. rep., National Hurricane Center. Available at https://www.nhc.noaa.gov/verification/pdfs/Verification_2021.pdf.
- Cangialosi JP, Blake E, DeMaria M, Penny A, Latta A, Rappaport E and Tallapragada V (2020) Recent progress in tropical cyclone intensity forecasting at the national hurricane center. *Weather and Forecasting* 35(5), 1913–1922. <https://doi.org/10.1175/WAF-D-20-0059.1>
- Dawid AP (1984) Present position and potential developments: Some personal views: Statistical theory: The prequential approach. *Journal of the Royal Statistical Society. Series A (General)* 147(2), 278–292.
- DeMaria M, Franklin JL, Onderlinde MJ and Kaplan J (2021) Operational forecasting of tropical cyclone rapid intensification at the national hurricane center. *Atmosphere* 12(6), 683. <https://doi.org/10.3390/atmos12060683>
- Duerr O, Sick B and Murina E (2020) *Probabilistic Deep Learning: With Python, Keras and TensorFlow Probability*, 1st edn. New York: Manning Publications.
- Foster D, Gagne DJ and Whitt DB (2021) Probabilistic machine learning estimation of ocean mixed layer depth from dense satellite and sparse in-situ observations. *Journal of Advances in Modeling Earth Systems* 13, e2021MS002474.

- Gal Y and Ghahramani Z** (2015) Dropout as a bayesian approximation: Representing model uncertainty in deep learning. <http://proceedings.mlr.press/v48/gal16.pdf>.
- Garg S, Rasp S and Thuerey N** (2022) WeatherBench probability: A benchmark dataset for probabilistic medium-range weather forecasting along with deep learning baseline models. [arXiv:2205.00865](https://arxiv.org/abs/2205.00865).
- Gneiting T, Balabdaoui F and Raftery AE** (2007) Probabilistic forecasts, calibration and sharpness. *Journal of the Royal Statistical Society: Series B (Statistical Methodology)* 69(2), 243–268. <https://doi.org/10.1111/j.1467-9868.2007.00587.x>
- Gneiting T and Katzfuss M** (2014) Probabilistic forecasting. *Annual Review of Statistics and Its Application* 1(1), 125–151. <https://doi.org/10.1146/annurev-statistics-062713-085831>
- Gordon EM and Barnes EA** (2022) Incorporating Uncertainty into a Regression Neural Network Enables Identification of Decadal State-Dependent Predictability in CESM2. *Geophysical Research Letters*. <https://doi.org/10.1029/2022gl098635>.
- Graves A** (2011) Practical variational inference for neural networks. In *Advances in Neural Information Processing Systems (NIPS)*, pp. 15–35. https://doi.org/10.1007/978-3-642-24797-2_3
- Guillaumin AP and Zanna L** (2021) Stochastic-deep learning parameterization of ocean momentum forcing. *Journal of Advances in Modeling Earth Systems* 13, e2021MS002534. <https://doi.org/10.1029/2021ms002534>
- Hamill TM** (2001) Interpretation of rank histograms for verifying ensemble forecasts. *Monthly Weather Review* 129(3), 550–560. [https://doi.org/10.1175/1520-0493\(2001\)129<0550:IORHFV>2.0.CO;2](https://doi.org/10.1175/1520-0493(2001)129<0550:IORHFV>2.0.CO;2)
- Hinton GE and Camp DV** (1993) Keeping the neural networks simple by minimizing the description length of the weights. In *16th Annual Conference On Learning Theory (COLT)*, pp. 5–13. <https://doi.org/10.1145/168304.168306>
- Jones MC and Pewsey A** (2009) Sinh-arcsinh distributions. *Biometrika* 96(4), 761–780.
- Jones C and Pewsey A** (2019) The sinh-arcsinh normal distribution. *Significance* 16(2), 6–7. <https://doi.org/10.1111/j.1740-9713.2019.01245.x>.
- Jospin LV, Laga H, Boussaid F, Buntine W and Bennamoun M** (2022) Hands-on bayesian neural networks – A tutorial for deep learning users. [arXiv:2007.06823v3](https://arxiv.org/abs/2007.06823v3).
- Kaplan J and Coauthors** (2015) Evaluating environmental impacts on tropical cyclone rapid intensification predictability utilizing statistical models. *Weather and Forecasting* 30(5), 1374–1396. <https://doi.org/10.1175/WAF-D-15-0032.1>.
- Kumaraswamy P** (1980) A generalized probability density function for double-bounded random processes. *Journal of Hydrology* 46(1–2), 79–88. [https://doi.org/10.1016/0022-1694\(80\)90036-0](https://doi.org/10.1016/0022-1694(80)90036-0)
- Landsea CW and Franklin JL** (2013) Atlantic hurricane database uncertainty and presentation of a new database format. *Monthly Weather Review* 141(10), 3576–3592. <https://doi.org/10.1175/MWR-D-12-00254.1>
- Mamalakis A, Ebert-Uphoff I and Barnes EA** (2022) Neural network attribution methods for problems in geoscience: A novel synthetic benchmark dataset. *Environmental Data Science* 1. <https://doi.org/10.1017/eds.2022.7>.
- McGovern A, Lagerquist R, Gagne DJ, Jergensen GE, Elmore KL, Homeyer CR and Smith T** (2019) Making the black box more transparent: Understanding the physical implications of machine learning. *Bulletin of the American Meteorological Society* 100(11), 2175–2199. <https://doi.org/10.1175/BAMS-D-18-0195.1>
- Mielke PW** (1975) Convenient beta distribution likelihood techniques for describing and comparing meteorological data. *Journal of Applied Meteorology* 14(6), 985–990. [https://doi.org/10.1175/1520-0450\(1975\)014<0985:cbdltf>2.0.co;2](https://doi.org/10.1175/1520-0450(1975)014<0985:cbdltf>2.0.co;2)
- Nipen T and Stull R** (2011) Calibrating probabilistic forecasts from an NWP ensemble. *Tellus Series A: Dynamic Meteorology and Oceanography* 63(5), 858–875. <https://doi.org/10.1111/j.1600-0870.2011.00535.x>
- Nix DA and Weigend A** (1994) Estimating the mean and variance of the target probability distribution. *Proceedings of 1994 IEEE International Conference on Neural Networks (ICNN'94)*. IEEE. <https://doi.org/10.1109/icnn.1994.374138>.
- Nix DA and Weigend AS** (1995) Learning local error bars for nonlinear regression. In Tesauro G, Touretzky DS and Leen TK (eds), *Advances in Neural Information Processing Systems 7 (NIPS94)*. Cambridge, MA: MIT Press, pp. 489–496.
- Sensoy M, Kaplan L and Kandemir M** (2018) Evidential deep learning to quantify classification uncertainty. [arXiv:1806.01768](https://arxiv.org/abs/1806.01768).
- Sountsov P, Suter C, Burnim J and Dillon JV** (2019) Regression with probabilistic layers in tensorflow probability. Available at <https://blog.tensorflow.org/2019/03/regression-with-probabilistic-layers-in.html>.
- Srivastava N, Hinton G, Krizhevsky A, Sutskever I and Salakhutdinov R** (2014) Dropout: A simple way to prevent neural networks from overfitting. *Journal of Machine Learning Research* 15(1), 1929–1958.
- Wen Y, Vicol P, Ba J, Tran D and Grosse R** (2018) Flipout: Efficient pseudo-independent weight perturbations on mini-batches. <https://arxiv.org/abs/1803.04386>
- Wikipedia Contributors** (2022) Skewness — Wikipedia, the free encyclopedia. Available at <https://en.wikipedia.org/w/index.php?title=Skewness&oldid=1070705103>.
- Wilson AG** (2020) The case for bayesian deep learning. [arXiv:2001.10995](https://arxiv.org/abs/2001.10995).

A. Appendix A

A.1. Sample sizes

Table of sample sizes for each basin and lead time for leave-one-out testing year 2020. AL denotes the Atlantic basin and EPCP denotes the Eastern/Central Pacific basin.

	Training	Validation	Testing
AL24	1,647	200	456
AL48	1,234	200	354
AL72	898	200	264
AL96	659	200	185
AL120	477	200	122
EPCP24	2,564	200	178
EPCP48	1,961	200	124
EPCP72	1,478	200	80
EPCP96	1,083	200	46
EPCP120	760	200	26

B. Appendix B

B.1. Sinh-arcsinh-Normal Formulations

B.1.1. Jones and Pewsey Formulation

B.1.1.1. Notation. The sinh-arcsinh-normal distribution was defined by Jones and Pewsey (2009). A more accessible, though less complete, presentation is given by Jones and Pewsey (2019). The following notation, which is used in this Appendix, is from the later paper:

- location $\zeta \in \mathbb{R}$,
- scale $\eta > 0$,
- skewness $\epsilon \in \mathbb{R}$,
- tailweight $\delta > 0$.

B.1.1.2. Distribution. Following Jones and Pewsey (2019), the sinh-arcsinh transformation of a random variable χ is defined as

$$S(\chi; \alpha, \beta) = \sinh(\beta \cdot \operatorname{asinh}(\chi) - \alpha). \tag{A.1}$$

A sinh-arcsinh-normal random variable X is defined as

$$X = \zeta + \eta \cdot S(Z; \epsilon, \delta), \tag{A.2}$$

where Z is a standard normal random variable. The probability density function of X is

$$f(x) = \frac{\delta}{\eta} \cdot \sqrt{\frac{1 + S^2(y; \epsilon, \delta)}{2\pi(1 + y^2)}} \cdot \exp\left(-\frac{1}{2}S^2(y; \epsilon, \delta)\right), \tag{A.3}$$

where

$$y = \frac{x - \zeta}{\eta}. \tag{A.4}$$

B.1.1.3. Moments. The first three moments of $S = S(Z; \epsilon, \delta)$ are derived in Jones and Pewsey (2009, p. 764) as

$$E(S) = \sinh(\epsilon/\delta) \cdot P_{1/\delta}, \tag{A.5}$$

$$E(S^2) = \frac{1}{2} [\cosh(2\epsilon/\delta) \cdot P_{2/\delta} - 1], \tag{A.6}$$

$$E(S^3) = \frac{1}{4} [\sinh(3\epsilon/\delta) \cdot P_{3/\delta} - 3 \sinh(\epsilon/\delta) \cdot P_{1/\delta}], \tag{A.7}$$

where

$$P_q = \frac{e^{1/4}}{\sqrt{8\pi}} \cdot [K_{(q+1)/2}(1/4) + K_{(q-1)/2}(1/4)] \tag{A.8}$$

and K is the modified Bessel function of the second kind.

B.1.1.4. Descriptive statistics. We compute the mean of X as

$$E(X) = E(\zeta + \eta \cdot S) \tag{A.9}$$

$$= \zeta + \eta \cdot E(S). \tag{A.10}$$

We compute the variance of X as

$$Var(X) = Var(\zeta + \eta \cdot S) \tag{A.11}$$

$$= \eta^2 \cdot Var(S) \tag{A.12}$$

$$= \eta^2 \cdot [E(S^2) - E(S)^2]. \tag{A.13}$$

We compute the skewness of X (also known as the third standardized moment) as

$$Skew(X) = \frac{E(X^3) - 3E(X)Var(X) - E(X)^3}{Var(X)^{3/2}}. \tag{A.14}$$

Wikipedia contributors (2022), where

$$E(X^3) = \zeta^3 + 3\zeta^2\eta E(S) + 3\zeta\eta^2 E(S^2) + \eta^3 E(S^3), \tag{A.15}$$

Beware: in general, $E(X) \neq \zeta$, $Var(X) \neq \eta^2$, and $Skew(X) \neq \epsilon$.

B.2. TensorFlow Formulation

B.2.1. Notation

TensorFlow includes the sinh-arcsinh-normal distribution as the default case of a more general family of transformed distributions implemented in the `tfp.distributions` package as `SinhArcsinh`. The notation used in TensorFlow is similar to the notation used by Jones and Pewsey, but the two are not identical:

- `loc` $\in \mathbb{R}$,
- `scale` > 0 ,
- `skewness` $\in \mathbb{R}$,
- `tailweight` > 0 .

Specifically, the words used by Jones and Pewsey are the same as the words used by TensorFlow, but the meanings of `scale` and `tailweight` are different. More on this below.

B.2.2. Distribution

TensorFlow defines the sinh-arcsinh-normal distribution somewhat differently than Jones and Pewsey. A sinh-arcsinh-normal random variable Y is defined as

$$Y = \text{loc} + \text{scale} \cdot F(Z). \tag{A.16}$$

where

$$F(Z) = \sinh([\sinh(Z) + \text{skewness}] \cdot \text{tailweight}) \cdot \frac{2}{F_0(2)} \tag{A.17}$$

and

$$F_0(2) = \sinh(\sinh(2) \cdot \text{tailweight}). \tag{A.18}$$

We compare (A.1) and (A.2) to (A.16), (A.17), and (A.18) to see that the two formulations are equivalent—that is, X and Y are equivalent random variables—if

$$\xi = \text{loc}, \tag{A.19}$$

$$\eta = \text{scale} \cdot \frac{2}{F_0(2)}, \tag{A.20}$$

$$\epsilon = \text{skewness}, \tag{A.21}$$

$$\delta = \frac{1}{\text{tailweight}}. \tag{A.22}$$

We note the likely source of confusion due to the descriptor “tailweight”. In Jones and Pewsey (2009), δ is said to “control the tailweight”, and in Jones and Pewsey (2019), δ is called the “tail weight parameter”. Nonetheless, δ is the reciprocal of the tailweight in TensorFlow.

B.3. Implementation

We substitute (A.21) and (A.22) into (A.5), (A.6), and (A.7) to compute the first three moments of S . The only modifications are

$$\epsilon/\delta = \text{skewness} \cdot \text{tailweight} \tag{A.23}$$

and

$$i/\delta = i \cdot \text{tailweight} \tag{A.24}$$

where $i \in \{1,2,3\}$. We compute the mean, variance, and skewness of Y using (A.10), (A.13), (A.14), and (A.15) by first computing¹

$$\eta = \text{scale} \cdot \frac{2}{\sinh(\sinh(2) \cdot \text{tailweight})} \tag{A.25}$$

and setting $\xi = \text{loc}$.

B.4. Notation in this paper

As our neural network implementation is based on TensorFlow, we follow the TensorFlow nomenclature in the body of this paper. For brevity, we introduce the following notation:

- $\mu = \text{loc}$,
- $\sigma = \text{scale}$,
- $\gamma = \text{skewness}$,
- $\tau = \text{tailweight}$.

Note: in general, $E(Y) \neq \mu$, $\text{Var}(Y) \neq \sigma^2$, and $\text{Skew}(Y) \neq \gamma$.

¹The TensorFlow Probability documentation for the sinh-arcsinh-normal distribution lists functions for mean, standard deviation, and variance, but they are not yet implemented in the library (v. 0.15.0). The code provided with this article fills this gap.